

1 **Multifractal spatial distribution of epilithic microphytobenthos on a**  
2 **Mediterranean rocky shore**

3 \*Martina Dal Bello<sup>1</sup>, Elena Maggi<sup>1</sup>, Luca Rindi<sup>1</sup>, Antonella Capocchi<sup>2</sup>, Debora Fontanini<sup>2</sup>, Carlos  
4 Sanz-Lazaro<sup>1,3</sup>, Lisandro Benedetti-Cecchi<sup>1</sup>

5 <sup>1</sup>Dipartimento di Biologia, Università di Pisa, CoNISMa, Via Derna 1, I-56126 Pisa, Italy

6 ([emaggi@biologia.unipi.it](mailto:emaggi@biologia.unipi.it), [lrindi@biologia.unipi.it](mailto:lrindi@biologia.unipi.it), [lbenedetti@biologia.unipi.it](mailto:lbenedetti@biologia.unipi.it))

7 <sup>2</sup>Dipartimento di Biologia, Università di Pisa, Via L. Ghini 5, I-56126 Pisa, Italy

8 ([acapocchi@biologia.unipi.it](mailto:acapocchi@biologia.unipi.it), [dfontanini@biologia.unipi.it](mailto:dfontanini@biologia.unipi.it))

9 <sup>3</sup>Present address: Departamento de Ciencias del Mar y Biología Aplicada, Universidad de  
10 Alicante, PO Box 99, E-03080 Alicante, Spain

11 ([carsanz@ua.es](mailto:carsanz@ua.es))

12 \* Corresponding author

13 Email: [mdalbello@biologia.unipi.it](mailto:mdalbello@biologia.unipi.it)

14 Tel. +39 050 221415

15 Fax. +39 050 2211410

16

17 Understanding how patterns and processes relate across spatial scales is one of the major goals in  
18 ecology.  $1/f$  models have been applied mostly to time series of environmental and ecological  
19 variables, but they can also be used to analyse spatial patterns. Since  $1/f$  noise may display scale-  
20 invariant behaviour, ecological phenomena whose spatial variability shows  $1/f$  type scaling are  
21 susceptible to further characterization using fractals or multifractals. Here we use spectral analysis  
22 and multifractal techniques (generalized dimension spectrum) to investigate the spatial distribution  
23 of epilithic microphytobenthos (EMPB) on rocky intertidal surfaces. EMPB biomass was estimated  
24 from calibrated colour-infrared images that provided indirect measures of rock surface chlorophyll  
25 *a* concentration, along two 8m and one 4m long transects sampled in January and November 2012.  
26 Results highlighted a pattern of spectral coefficient close to or greater than one for EMPB biomass  
27 distribution and multifractal structures, that were consistent among transects, implying scale-  
28 invariance in the spatial distribution of EMPB. These outcomes can be interpreted as a result of the  
29 superimposition of several biotic and abiotic processes acting at multiple spatial scales. However,  
30 the scale-invariant nature of EMPB spatial patterns can also be considered a hallmark of self-  
31 organization, underlying the possible role of scale-dependent feedback in shaping EMPB biomass  
32 distribution.

33

34 The measurement of variability in population abundance and distribution followed by the  
35 identification of the underlying causes are major goals in ecology (Denny et al. 2004). Hierarchical  
36 sampling designs, combined with variance components estimates, have been extensively employed  
37 to examine spatial patterns in abundance of animal and plant populations, showing how most of the  
38 variation is concentrated at small scales (Fraschetti et al. 2005, Meyer 2006). These methods focus  
39 on discrete spatial scales and require decisions to be made about the number, extent and spacing of  
40 the scales investigated. A possible limitation of this approach is that important scales of variation  
41 may be omitted from the study. The major strength of hierarchical sampling designs is that they  
42 enable the simultaneous analysis of a broad range of scales and they are the only possible approach  
43 to compare biogeographic or continental scales or when the habitat of interest (e.g., rocky shores) is  
44 interspersed among unfavourable habitats (e.g., sandy beaches). The alternative approach of  
45 sampling continuously in space is simply impractical in these circumstances.

46 Examining spatial variation in ecological variables continuously in space may, however,  
47 capture patterns of variability that could go undetected otherwise. For example, Denny et al. (2004)  
48 quantified spatial variation of physical and biological variables sampling continuously along three  
49 intertidal transects tens to hundreds of meters in length, on a wave-swept rocky shore at Hopkins  
50 Marine Station (CA). Results contradicted the expectation that variability is concentrated mostly at  
51 small spatial scales and the existence of a characteristic scale of variability. In contrast, using  
52 spectral analysis, these authors found a continuous increase of variance with the scale of  
53 observation, a pattern that was well described by  $1/f$ -noise models. One of the key findings of this  
54 work was that, for several of the variables analyzed, patterns of distribution were adequately  
55 described by a power law with a spectral coefficient close to one. These patterns are usually  
56 referred to as 'pink noise' and underscore variability at all the scales analyzed, suggesting that  
57 multiple processes affect the response variable of concern.

58 Pink noise patterns of variability can be further characterized using fractals (Halley and  
59 Incausti 2004). Mandelbrot (1983) coined the term “fractal” to designate objects with fractional or a  
60 non integer number of dimensions, that display self-similarity across a range of spatial scales of  
61 observations. Fractal methods have been applied to various natural phenomena, including patterns  
62 in surface topography (Commito and Rusignuolo 2000), blood networks (Yang and Wang 2013),  
63 climatic variation (Bodai and Tel 2012), earthquakes (Malamud and Turcotte 1999) and fires  
64 (Abaimov et al. 2007). All these phenomena are usually described by one estimated fractal  
65 dimension  $D$ , which measures the object’s capacity to fill the space. In some cases, however, the  
66 description of particular natural events requires not one, but a set of fractal dimensions. These  
67 phenomena are better characterized by multifractals, which can be seen as sets of interweaved  
68 fractals with different dimensions (Stanley and Meakin 1988). Multifractals are useful for the  
69 description of the spatial (or temporal) organization of population abundance or biomass for which  
70 complex patterns are expected (Halley et al. 2004). Multifractality is attributed to long-range  
71 correlations and thus should be expected in the presence of  $1/f$  noise spatial (or temporal) patterns  
72 (Stanley and Meakin 1988). Moreover, multifractal analysis provides a complementary approach to  
73 spectral analysis. While spectral analysis examines the relative contribution of different spatial or  
74 temporal scales to total variance and may detect scale-invariant patterns, multifractals evaluate  
75 whether scaling relations change according to the spatial or temporal resolution of observations.  
76 Overall,  $1/f$  noise and multifractality are related to the extent that both patterns may reflect the  
77 juxtaposition of multiple independent processes (Kendal 2013). However, the combined action of  
78 multiple processes is not the only mechanism involved in the formation of power law distributions.  
79 Borda-de-Água and co-authors (2007), simulating the spatial distribution of model tree species,  
80 found that multifractals may also originate from Lévy flight dispersal patterns, with long distance  
81 events being frequent enough to generate a fat tail in the frequency distribution of dispersal  
82 distances.

83 Epilithic microphytobenthos (EMPB) forming biofilms on rocky shores are ubiquitous  
84 worldwide and consist primarily of photosynthetic organisms, such as diatoms, cyanobacteria and  
85 macroalgal spores and germlings (Hill and Hawkins 1991). Biofilms play important functional roles  
86 on rocky intertidal shores, facilitating the attachment of algal propagules and the settlement of  
87 larvae of many sessile invertebrates (Rodriguez et al. 1993) and providing food for grazing  
88 gastropods (Underwood 1984). EMPB constitutes the major fraction of biomass produced and  
89 directly consumed on a rocky shore (Thompson et al. 2000).

90 EMPB offer unique opportunities to investigate the spatial ecology of rocky shore populations.  
91 The microscopic size of constituting organisms enables the analysis of a broad range of tractable  
92 scales, from very small (mm) to very large (tens to hundreds of meters) for the organisms of  
93 concern. Recent advances in field-based remote sensing, in particular colour-infrared imagery  
94 (CIR), have significantly improved our ability to obtain *in situ* quantitative measures of chlorophyll  
95 *a* (a proxy for EMPB biomass) enabling the collection of large amount of data at a fine spatial  
96 resolution and over a range of several, continuous spatial scales (Murphy et al. 2006). Hence data  
97 can be analyzed across the entire range of spatial scales within the boundary of an image or a set of  
98 consecutive images and the relative positions of observations are implicitly stored within the images  
99 (Murphy et al. 2009).

100 Notwithstanding rapid technological progress enabling efficient sampling of intertidal biofilms,  
101 to date only one study has examined variability of EMPB at multiple spatial scales (Murphy et al.  
102 2008). Using a hierarchical sampling design and block mean square analysis, Murphy et al. (2008)  
103 showed how variability in EMPB biomass was low at small spatial scales (block sizes from 0.002 to  
104 2.26 cm<sup>2</sup>), but increased with increasing block-size up to the largest scale examined (36.19 cm<sup>2</sup>).  
105 Because variation increased with the scale of observation and different processes were invoked to  
106 explain these patterns, the results of Murphy et al. (2008) may indeed underscore  $1/f$  noise process  
107 and, possibly, multifractal structure in EMPB distribution. Indeed, multifractals have been detected  
108 in a study on the spatial distribution of soft bottom microphytobenthos (Seuront and Spilmont 2002)

109 and in a periphyton community at different stages of succession in experimental tanks (Saravia et al.  
110 2012). In particular, Saravia and co-authors, found that scale invariance arose at each stage of  
111 succession, thus highlighting a temporally consistent scale-invariant behaviour that was ascribed to  
112 self-organization. In this paper we examine spatial variation in EMPB biomass on rocky intertidal  
113 shores in the Northwest Mediterranean by means of colour-infrared imagery. From the results of  
114 previous studies on the spatial distribution of microphytobenthos (Seuront and Spilmont 2002,  
115 Murphy et al. 2008, Saravia et al. 2012) we test the following hypotheses: (1) the spectral  
116 decomposition of spatial variance in EMPB abundance follows a power law; (2) the distribution of  
117 EMPB in 2-dimensional space is multifractal. We test these hypotheses applying spectral analysis  
118 and multifractal geometry to nearly-continuous spatial EMPB data under natural field conditions.

## 119 **Methods**

### 120 **Study system**

121 The study was done along the coast of Calafuria (Livorno, 43°30' N, 10°19' E) between January and  
122 November 2012. The coast is composed of gently sloping sandstone platforms with high-shore  
123 levels (0.3-0.5 m above mean low-level water) characterized by assemblages of barnacles  
124 interspersed among areas of seemingly bare rock, where EMPB develops. Calafuria's EMPB  
125 assemblages prevalently comprise cyanobacteria and diatoms. At this height on the shore, the main  
126 grazers are the littorinid snails *Melarhappe neritoides* (L.), which aggregate in pits and crevices  
127 when the substratum is dry and forage during sea storms and rain events (Skov et al. 2010 and  
128 references therein). The only other grazer that can occasionally forage at these heights of the shore  
129 is the limpet *Patella rustica* (L.).

### 130 ***In situ* estimates of chlorophyll *a***

131 Following the image-based method proposed by Murphy et al. (2006), chlorophyll *a*, which is used  
132 as a proxy for biofilm biomass, was estimated from a ratio of reflectance at near-infrared (NIR) and  
133 red bands (Jordan 1969). The NIR:red ratio (Ratio Vegetational Index - RVI) detects the absorption

134 of chlorophyll *a* using the reflectance at NIR wavelengths, where chlorophyll *a* does not absorb,  
135 normalized by the reflectance at red wavelengths (corresponding to the peak of chlorophyll *a*  
136 absorbance) (Murphy et al. 2006).

137 Here we used a particular IR-sensible camera (ADC, Tetracam Inc.), commonly employed in  
138 agricultural and vegetational studies, to obtain chlorophyll *a* estimates. The ADC is a single sensor  
139 digital camera designed and optimized to capture visible light wavelengths longer than 520 nm and  
140 near-infrared wavelengths up to 920 nm. This camera uses a Bayern-pattern filter to produce a 3-  
141 layered photo comprising green, red and NIR layers which are analogous to the red, green and blue  
142 layers produced by conventional digital cameras. The ADC system writes a greyscale RAW file for  
143 every photo; hence every photo has been colour-processed and recorded in TIFF format, using the  
144 program PixelWrench 2, prior to further use (Agricultural Camera User's Guide 2010). Photos are  
145 2560 by 1926 pixels in size and cover an area of ground of about 52 x 35 cm. The approximate  
146 spatial resolution of each pixel is 0.2 mm.

147 In order to get the best focus, photos were acquired using a stable platform 60 cm above and  
148 normal to the rock surface. Different exposure times for each photo were selected depending on  
149 ambient light conditions, in order to produce bright but not saturated photos. To calibrate pixel  
150 values to the varying light conditions and different camera settings, a reflectance standard of 30%  
151 reflective Spectralon®, representing the range of brightness of Calafuria rock surfaces with  
152 microalgae, was always placed within the field of view of the camera. The calibration of data to  
153 reflectance is obtained normalizing pixel values of each band to the brightness of pixels over the  
154 standard (see Supplementary material Appendix 1).

155 All methods of collecting remotely sensed data require calibration/validation by comparison  
156 with direct measurements (Murphy et al. 2005). In order to calibrate/validate estimates of  
157 chlorophyll *a* derived from the ADC data, 100 rock chips ~2 cm in diameter were removed by  
158 cutting the rock with a diamond corer powered by a petrol driller and then photographed using the  
159 ADC camera. Rock chips were then taken to the laboratory for the determination of the amount of

160 chlorophyll *a*, which was extracted in methanol as in Thompson et al. 1999. Laboratory  
161 measurements of chlorophyll *a* were related to ADC estimates (RVI index) using least squares  
162 linear regression.

### 163 **Sampling and data analysis**

164 Spatial patterns of EMPB abundance were investigated along two 8m transects and one 4m transect  
165 about 50m from each other, yielding 18 and 9 ADC photos per transect, respectively. Sampling was  
166 repeated in January and November 2012.

167 The photographs obtained from each individual transect were stitched to form a composite  
168 image using a photogrammetric software (Kolor Autopano Giga 2.6). The area of the rock included  
169 in each individual photo was delimited with white chalk at its corners before sampling. Adjacent  
170 photos overlapped at their margins and the region of overlap was indicated by the white chalk  
171 marks. This procedure facilitated the alignment of photos in the composite image, but resulted in  
172 non-continuous spatial series of data because spurious chlorophyll *a* values can originate from the  
173 interpolation method (nearest neighbour) used by the photogrammetric software to merge pixels in  
174 the regions of overlap. Three series of observations were extracted from each composite image,  
175 where a series consisted of a set of points one pixel in height and arranged along a common 'y'  
176 coordinate (Fig. 1B). Each series had gaps corresponding to the areas in which adjacent photos  
177 overlapped; for each series, the size of gaps was determined by measuring the distance in pixels  
178 between each set of continuous points in the composite image (grey lines in Fig. 1B). The extracted  
179 data were then processed with a java-routine in the ImageJ program in order to quantify NIR/red  
180 ratios (the RVI index) that were then transformed into estimates of chlorophyll *a* concentration at  
181 the pixel scale. Pixel per pixel calibration to reflectance is part of this routine (Supplementary  
182 materials Appendix 1).

183 We used spectral analysis on linearly detrended data for each spatial series of chlorophyll *a*  
184 estimates to characterize the spatial patterns of variation in EMPB biomass along each series of data



185 within each transect. Although our series were unevenly spaced, knowing the size of gaps enabled  
186 us to use the Lomb-Scargle algorithm (Lomb 1976, Scargle 1982) modified by Press et al. (1992)  
187 for spectral analysis. Spectral densities were estimated between the fundamental and the Nyquist  
188 frequency. The fundamental frequency is defined as  $1/x_{\max}$ , where  $x_{\max}$  is the maximum spatial  
189 extent of the data, corresponding to transects of either 4 or 8 m in our study. The Nyquist frequency  
190 is defined as  $1/2\Delta x$ , where  $\Delta x$  is the average distance between the irregularly spaced sampling  
191 points. We smoothed the periodogram with Hamming window = 10, thus minimizing the loss of  
192 information at higher frequencies (Chatfield 2004). The spectral density estimate for each series,  
193  $S(f)$ , was then plotted against frequency of observation on a natural log-log scale and the spectral  
194 coefficient ( $\beta$ ) was determined as the slope of the regression changed of sign (e.g., Denny et al.  
195 2004).  $\beta$ s were estimated within the range of frequencies that displayed a  $1/f$  noise pattern: the  
196 Nyquist and -7 (on the natural logarithm scale). We truncated the series at -7 because at larger  
197 spatial scales (lower frequencies) the spectral densities deviated from a  $1/f$  noise pattern, becoming  
198 more similar to an autoregressive process. This behaviour possibly reflected the decreasing number  
199 of observations available to estimate spectral densities with increasing scale of observation.

200 The previous analysis used EMPB biomass values at the resolution of the pixel that were  
201 calibrated against laboratory measurements of chlorophyll concentration obtained from sandstone  
202 cores with areas corresponding to approximately 6400 pixels. This mismatch between the resolution  
203 at which the RVI and chlorophyll measurements were obtained might lead to biased estimates of  
204 spectral coefficients due to error propagation and the noise generated by the camera. To assess this  
205 potential bias we performed a further spectral analysis on nearly continuous spatial series of EMPB  
206 biomass data obtained from non-overlapping quadrats of 80 x 80 pixels (6400 pixels) extracted  
207 from the stitched image of each transect along a common y coordinate. The average spectral  
208 coefficients obtained for each transect with the two methods were then compared with a paired t-  
209 test.

210 To test the hypothesis that the spatial distribution of EMPB was multifractal, a total of 39 plots  
211 of 1024 by 1024 pixels each (approximately 400 cm<sup>2</sup>) were selected from all the transects and  
212 processed with the java-routine on ImageJ program to obtain EMPB biomass estimates for each  
213 pixel. This plot size was chosen to match as closely as possible the range of scales employed in the  
214 spectral analysis, where the largest scale of -7 corresponded to about 1096 pixels in length.  
215 Multifractal geometry was determined following the method proposed by Saravia *et al.* (2012) to  
216 estimate the generalized dimensions spectrum  $D_q$  of each plot (see Supplementary material  
217 Appendix 2 for formulae and details of calculation).  $D_q$  is related to the spatial arrangement of  
218 biomass, computed in the algorithm as the partition function  $Z_q$ , and reflects the patterns of change  
219 that occur when zooming in or out from each plot by steps of size  $\epsilon$ . The exponent  $q$  in the  
220 algorithm (chosen by the investigators) captures spatial variation in high or low values of biomass  
221 depending on its value (here, we used  $q$  values from -20 to +20). When  $q$  is a relatively large  
222 positive number,  $D_q$  reflects the spatial patterns of large biomass values (chlorophyll  $a > 1 \mu\text{g}/\text{cm}^2$ ),  
223 whereas when  $q$  is a large negative number,  $D_q$  describes the spatial pattern of small biomasses  
224 (chlorophyll  $a$  estimates between 0 and  $1 \mu\text{g}/\text{cm}^2$ ).

225 For multifractal objects, the spectrum of generalized dimensions  $D_q$  (not to be confounded  
226 with the power spectrum) takes the shape of a sigmoid curve and it is a decreasing function of  $q$   
227 (Grassberger 1983). For mono- or non-fractal objects the spectrum is a non decreasing function of  
228  $q$ . The other assumption that must be met for the biomass distribution to be multifractal is that the  
229 relationship  $\log(Z_q)$  versus  $\log(\epsilon)$  should be linear for all the  $q$  used in the calculation of  $D_q$  (see  
230 Supplementary material Appendix 2).

231 Deviations from spatially homogeneous biomass distributions are quantified as positive and  
232 negative deviations from 2 (the expected value of the exponent of a non-fractal 2D space), for low  
233 and high biomass values respectively. A plot with high peaks of biomass will have increasingly  
234 lower  $D_q$  for positive  $q$  and a plot with sharp collapses of biomass will have increasingly larger  $D_q$

235 for negative  $q$ . A plot with both peaks and falls will show large deviations from 2 (Saravia et al.  
236 2012).

237 To further characterize spatial patterns of EMPB distribution we examined how  $D_I$  varied  
238 along transects, sampling dates and potentially important environmental drivers.  $D_I$  is directly  
239 related to Shannon entropy and can be thought as the decrease in information content when  
240 increasing box size in the box counting method (Mendoza et al. 2010). Large values of  $D_I$  indicate  
241 greater homogeneity with increasing box size, while low values indicate the opposite. To obtain  
242 reasonably long spatial series of  $D_I$  values along transects, we repeated the multifractal geometry  
243 analysis described above using plots of 128 x 128 (instead of 1024 x 1024) pixels from the two 8m  
244 transects. These plots were aligned along a common 'y' coordinate along composite images and the  
245 size of gaps was recorded as the number of missing 128 x 128 plots in the regions of overlap  
246 between adjacent photos (Fig. 1C). This yielded a series of 64  $D_I$  values for each 8m transect and  
247 sampling date. We analysed these data in two ways. First, we used a mixed-effect model including  
248 the main effects and interactions among densities of grazers (the littorinid *Melaraphe neritoides*),  
249 number of pits and average rainfall in the week before sampling in the fixed part of the model, and  
250 transects as a grouping factor with a random intercept. Densities of grazers and the number of pits  
251 were calculated within each individual image of the composite transects, whereas daily precipitation  
252 data were obtained from Lamma Toscana (<http://www.lamma.rete.toscana.it/>). Rainfall and aerial  
253 temperature were the two of most obvious environmental variables discriminating between  
254 sampling dates. The daily values of these variables were highly correlated in the week before  
255 sampling ( $r=0.9$ ,  $n=7$ ), so we used only rainfall in the analysis because this variable has been related  
256 to the activity of grazers in previous studies (Bates and Hicks 2005, Skov et al. 2010).

257 Following the results of the mixed effect model, which highlighted a significant grazer x  
258 rainfall interaction (see Results), we examined the cross-correlation between  $D_I$  and density of  
259 grazers along each transect at each date of sampling. We used the function `spline.correlog` in the R  
260 package 'ncf' for this analysis (Bjornstad and Falck 2001).

261 All analyses were performed in R 2.15.2. (R Development core team 2012).

## 262 **Results**

263 There was a strong linear relation between chlorophyll *a* estimates obtained with laboratory  
264 extraction methods and the RVI index (Fig. 2;  $R^2 = 0.80$ ,  $SE = 0.12$ ,  $p < 0.001$ ,  $n = 100$ ), indicating that  
265 ADC images can be used to predict EMPB abundance.

266 Variance of chlorophyll *a* concentration was inversely related to the frequency of observation  
267 for all the spatial series investigated, (see Appendix 3 Fig. A3.1 and A3.2). Spectral coefficients  
268 ranged from 0.95 to 1.64 (mean 1.34), indicating a predominance of “red-noise” spectra (Table 1).  
269 The analysis based on quadrats of 80 x 80 pixels yielded very similar results to those obtained from  
270 the analysis of series of individual pixels, with spectral coefficients in the range 0.86 -1.7 that were  
271 still indicative of ‘red-noise’ spatial patterns (Table A4.1, Supplementary material Appendix 4).  
272 **The paired *t*-test did not highlight statistically significant differences in mean spectral coefficients**  
273 **between scales calculated at the transect level ( $t = -1.36$ ,  $P > 0.23$ , with five degrees of freedom).**

274 EMPB biomass displayed multifractal spatial distribution in all plots of 1024 x 1024. The  
275 theoretical prediction that  $D_q$  should be a monotonically decreasing function of  $q$  was supported in  
276 all cases (Fig. 3) and the linear relation necessary for the biomass distribution to be multifractal was  
277 achieved for all the plots sampled and all the values for  $q$  used to calculate the spectrum of  
278 generalized dimensions ( $R^2$  were larger than 0.99 in all cases) (see Supplementary material  
279 Appendix 2, Fig. A2.1).

280 Multifractal spatial distribution of EMPB biomass also emerged from the analysis of the plots  
281 of 128 x 128 pixels (data not shown). The analysis of the resulting  $D_I$  values highlighted a  
282 statistically significant interactive effect of the density of snails and the average rainfall in the week  
283 before sampling (Table 2).  $D_I$  decreased with increasing density of grazers under dry  
284 meteorological conditions, whereas the opposite was observed under wet conditions (Fig. 4).

285 The spatial correlograms showed a positive relation between  $D_I$  and littorinid density at small  
286 spatial scales for all combinations of transects and sampling dates (Fig. 5). Positive cross-  
287 correlation was also evident at the largest spatial scale in one of the two transects sampled in  
288 November 2012 (Fig. 5).

## 289 **Discussion**

290 We found a strong linear relation between laboratory chlorophyll *a* estimates and the RVI index.  
291 The regression model explains 80% of variability in the data. Microscopic variations in colour and  
292 topography of the surface of sandstone rock cores, together with occasional small areas of specular  
293 reflectance likely accounted for some of the remaining 20% of unexplained variability (Murphy et  
294 al. 2009).

295 Our results support the hypothesis that EMPB biomass is distributed according to a power law  
296 and that multifractal organization characterizes EMPB spatial distribution. Spectral coefficients for  
297 all the series of observations taken along linear transects were **close to or greater than one**.  
298 Expanding the analysis in a two-dimensional space through multifractal geometry produced an  
299 analogous outcome. Multifractal analysis, indeed, indicated that the spatial distribution of EMPB  
300 was characterized by a combination of several fractal sets with different fractal dimensions. The  
301 scale-invariant nature of EMPB biomass distribution suggests the superimposition of several abiotic  
302 and biotic processes operating at different spatial scales (Hausdorff and Peng 1996). Positive and  
303 negative biotic interactions are likely to be responsible for the variability observed at the smallest  
304 spatial scales (from millimetres to centimetres). For example, the production of extracellular  
305 polymeric substances (EPS) has been described as a mechanism of facilitation between microalgal  
306 cells that may promote the development of EMPB patches, through reducing desiccation, favouring  
307 nutrient retention and providing protection from UV radiations (Potts 1999). However, within  
308 EMPB patches mechanisms of facilitation could be counterbalanced by competitive interactions for  
309 resources such as light, nutrients and space among microalgae. These mechanisms of facilitation

310 and competition may further interact with the microtopography of substratum, which may also have  
311 a multifractal structure (Commito and Rusignuolo 2000) and can promote variation in important  
312 variables for EMPB growth, such as solar radiation, ground temperature and moisture (Murphy et  
313 al. 2008). For example, the presence of small pits and crevices on the rock favours water retention,  
314 providing a surrounding halo of favourable conditions for the development of EMPB (Jackson et al.  
315 2013).

316 Superimposed to these processes there is the effect of grazers (Thompson et al. 2004), whose  
317 foraging activity is known to influence either positively or negatively EMPB biomass distribution.  
318 The most important grazer at the study site was *Melarhappe neritoides*, which actively forage on  
319 EMPB, leaving characteristic halos deprived of microalgae. Generally the exclusion of littorinid  
320 grazers from plots of rocky substratum resulted in short-term increases of EMPB growth (Stafford  
321 and Davies 2005). However, once EMPB biomass is monitored for longer periods, as in Skov et al.  
322 2010, the initial positive effect of excluding snails turns out to be negative. A history of grazing by  
323 *M. neritoides* can boost EMPB growth by continuously removing detritus and dead cells and, thus,  
324 favouring light penetration and nutrient access.

325 Our results support the view that grazing activity is mediated by physical processes linked to  
326 fresh water supply. Littorinids are more active in moist conditions, so that their impact on EMPB  
327 biomass may be larger during wet days, regardless of their density (Bates and Hicks 2005). We  
328 found a general positive association between grazers and  $D_I$  at small spatial scales, suggesting that  
329 grazers may generate homogenous areas of low biomass in their neighbourhoods under different  
330 environmental conditions (larger  $D_I$  values correspond to lower disorder). This positive association  
331 may occasionally extend at larger scales, as observed in one transect in November 2012. However,  
332 the mixed-effect model also suggested that grazing activity may result in more heterogeneous  
333 spatial patterns of distribution of EMPB biomass in wet compared to dry conditions and that the  
334 relation between  $D_I$  and density of grazers is negative in the dry sampling date (January 2012) and  
335 slightly positive in the wet sampling date (November 2012). Although we cannot exclude that

336 factors other than rainfall differed between sampling dates, our results strongly suggest that rainfall  
337 mediates not only the effect of grazers on mean EMPB biomass, as described in other studies (Bates  
338 and Hicks 2005, Stafford and Davies 2005, Skov et al. 2010), but also the spatial organization of  
339 EMPB distribution.

340 Yet, spatial self-organization may provide an alternative way to interpret our results. Spatial  
341 self-organization embraces a set of dynamical processes for which large-scale ordered spatial  
342 patterns and power law clustering distributions arise from local interactions between the  
343 components of a system (Solé and Bascompte 2006). The unifying ecological principle invoked to  
344 explain these patterns is the presence of scale-dependent feedback, which emerges mainly from  
345 short-range facilitation through habitat modification and long-range competition for resources. The  
346 way this feedback acts follows Turing's scale-dependent activator-inhibitor principle (Rietkerk and  
347 van de Koppel 2008). Evidences of spatial patterns linked to scale-dependent feedback have been  
348 found in a variety of ecosystems, ranging from arid habitats (Rietkerk et al. 2002) to intertidal  
349 mudflats (Weerman et al. 2010) and mussel beds (van de Koppel et al. 2005). The power law  
350 clustering distribution of EMPB biomass that resulted in our study may underscore self-  
351 organization (Pascual et al. 2002). In EMPB communities, biofilm formation through EPS  
352 production by microalgae could be able to trigger the scale-dependent feedback required for the  
353 formation of a self-organizing pattern. Specifically, the short distance interactions of mutual  
354 benefits between microalgal cells and the large distance competitive processes for resources  
355 described before could be seen as, respectively, the activators and inhibitors of Turing's principle.  
356 In the perspective of self-organization, the strength of positive and negative feedbacks is able to  
357 mediate the action of environmental processes through mechanisms of resource concentration that  
358 take place in the activator-inhibitor systems mentioned before (Rietkerk and van de Koppel 2008).  
359 For example, across intertidal mudflats, erosive losses of microalgae by tidal flows are dampened  
360 by EPS. In a similar manner, in EMPB systems, the negative effects of adverse environmental

361 conditions (temperature, insolation, dryness) could be mediated by EPS, which act both locally and  
362 at larger scales concentrating resources and alleviating desiccation and insolation stress.

363 Positive feedbacks associated with EPS were also suggested by the change in scaling regime  
364 that was evident in some of the power spectra, where the negative relation between variance and  
365 scale of observation became steeper at frequencies greater than -2.5 (on the logarithm scale). This  
366 indicated a change in autocorrelation at very small spatial scales, possibly reflecting the presence of  
367 small patches of EMPB biomass maintained by positive species interactions. The exact mechanisms  
368 underlying the observed change in scaling regime remain open to further scrutiny.

369 Our results have important methodological implications, emphasizing the importance of high-  
370 frequency sampling to fully capture the patterns of variability and organization of ecological  
371 variables. *In situ* remote sensing techniques facilitate this task, resulting in a large amount of data  
372 that can be analysed using multiple statistical techniques. The possibility of integrating different  
373 analytical approaches enabled us to support the hypothesis that  $1/f$  noise spatial patterns are also  
374 multifractal. These results can be interpreted from two different, but not mutually exclusive  
375 perspectives. Both interpretations stress the importance of local biotic interactions, either positive or  
376 negative, in shaping spatial pattern of distribution of EMPB biomass, while differing in the way  
377 environmental processes are supposed to affect microalgal abundance. One interpretation is that  
378 environmental processes associated with temperature, insolation and moisture exert a direct effect  
379 on EMPB, determining relatively large scale variation in its biomass. In contrast, under self-  
380 organization, the influence of these abiotic variables is indirect, being mediated by the presence of  
381 the EPS matrix in which microalgal cells are embedded.

382 Although we did not analyze this fact, the combined use of spectral and multifractal techniques  
383 suggests, in some cases, the existence of two scaling regimes in the spatial distribution of EMPB  
384 biomass along transects. Visual inspection of a number of power spectra, indeed, could highlight  
385 that high frequencies (i.e., small spatial scales) have a higher spectral coefficient and low



386 frequencies (i.e., large spatial scales) a lower one. Temporal tracking of changes in patch size could  
387 help discriminating between contrasting exogenous and endogenous processes influencing EMPB  
388 distribution (Manor and Shnerb 2008). If, in a time series of patch size variation the probability that  
389 patches shrink within a fixed time span decays exponentially with their size, the observed spatial  
390 structure can be ascribed mostly to the action of physical processes, such as the topographic  
391 complexity of the substratum (Vandermeer et al. 2008). If patch shrinking scales logarithmically  
392 with patch size, grazing could play a major role in the clustering process (as in Kefy et al. 2007).  
393 Conversely, if endogenous positive feedbacks are responsible for power law cluster distribution,  
394 large clusters should disappear with a rate that depends linearly on patch size (Vandermeer et al.  
395 2008). Ultimately, manipulative experiments will be required to evaluate the importance of self-  
396 organization and the influence of external physical and biological processes in determining spatial  
397 patterns in EMPB distribution.

398 *Acknowledgements* – We sincerely thank A. Mascellani for the support with ImageJ software and  
399 several students for help with fieldwork. This work is part of a requirement for a PhD by M. Dal  
400 Bello and was partially supported by the University of Pisa and by the FP 7 EU project VECTORS  
401 “VECTORS of Change in Oceans and Seas Marine Life, Impact on Economic Sectors”. CS was  
402 supported by a postdoctoral grant from the Alfonso Martin Escudero Foundation from Spain.

403

404 **References**

- 405 1. Abaimov, S. G., et al. 2007. Recurrence and interoccurrence behavior of self-  
406 organized complex phenomena. – *Non linear processes in geophysics* 14(4): 455–464.
- 407 2. Agricultural Camera User’s Guide. Documentation Copyright 2010 Tetracam Inc,  
408 21601 Devonshire Street Suite 310 Chatsworth, CA 91311 USA.
- 409 3. Bates, T. W. and Hicks, D. W. 2005. Locomotory behaviour and habitat selection in  
410 littoral gastropods in Caribbean limestone shores. – *J. Shellfish Res.* 24(1): 75–84.
- 411 4. Bjornstad, O. N. And Falck, W. 2001. Non-parametric spatial covariance functions:  
412 estimation and testing. – *Environ. Ecol. Stat.* 8: 53–70.
- 413 5. Bodai, T. And Tel, T. 2012. Annual variability in a conceptual climate model:  
414 Snapshot attractors, hysteresis in extreme events, and climate sensitivity. – *Chaos* 22(2):  
415 023110.
- 416 6. Borda-de-Água, L. et al. 2007. Scaling biodiversity under neutrality. – In: Storch, D.  
417 et al. (ed.), *Scaling Biodiversity*. Cambridge Univ. Press, pp. 347–375.
- 418 7. Chatfield, C. 2004. *The analysis of time series: an introduction*. 6<sup>th</sup> edition. – CRC  
419 Press, Boca Raton, Florida, USA.
- 420 8. Commito, J. A. And Rusignuolo B. R. 2000. Structural complexity in mussel beds:  
421 the fractal geometry of surface topography. – *J. Exp. Mar. Biol. Ecol.* 255: 133–152.
- 422 9. Denny, M. W. et al. 2004. Quantifying scale in ecology: lessons from a wave swept  
423 shore. – *Ecol. Monog.* 74: 513–532.
- 424 10. Frascchetti, S. et al. 2005. Patterns of distribution of marine assemblages from rocky  
425 shores: evidence of relevant scales of variation. – *Mar. Ecol. Prog. Ser.* 296: 13–29.
- 426 11. Grassberger, P. 1983. Generalized dimensions of strange attractors. – *Phys. Lett.* 97:  
427 227–230.

- 428 12. Halley, J. M. and Inchausti, P. 2004. The increasing importance of  $1/f$  noises as  
429 models of ecological variability. – *Fluctuation and Noise Letters* 4(2): R1–R26.
- 430 13. Halley, J. M. et al. 2004. Uses and abuses of fractal methodology in ecology. – *Ecol.*  
431 *Lett.* 7: 254–271.
- 432 14. Hausdorff, J. M. and Peng, C. -K. 1996. Multiscale randomness: A possible source of  
433 noise in biology. – *Phys. Rev.* 54(2): 2154–2157.
- 434 15. Hill, A. S. and Hawkins, S. J. 1991. Seasonal and spatial variation on epilithic  
435 microalgae distribution and abundance and its ingestion by *Patella vulgata* on a moderately  
436 exposed rocky shore. – *J. Mar. Biol. Ass. UK* 71: 403–423.
- 437 16. Jackson, A. C. et al. 2013. Biofilms on rocky shores: Influence of rockpools, local  
438 moisture and temperature. – *J. Exp. Mar. Biol. Ecol.* 443: 46–55.
- 439 17. Jordan, C. F. 1969. Derivation of leaf area index from quality of light on the forest  
440 floor. – *Ecology* 50: 663–666.
- 441 18. Kefy, S. et al. 2007. Spatial vegetation patterns and imminent desertification in  
442 Mediterranean arid ecosystems. – *Nature* 449: 213–217.
- 443 19. Kendal W. S. 2013. Fluctuation scaling and  $1/f$  noise. – *J. Basic Appl. Phys.* 2(2):  
444 40–49.
- 445 20. Lomb, N. R. 1976. Least-squares frequency analysis of unequally spaced data. –  
446 *Astrophys. Space Sci.* 39: 447–462.
- 447 21. Malamud, B. D. and Turcotte, D. L. 1999. Self-organized criticality applied to  
448 natural hazards. – *Nat. Hazards* 20(2–3): 93–116.
- 449 22. Mandelbrot, B. 1983. *The Fractal Geometry of Nature*. – Freeman (Eds).
- 450 23. Manor, A. and Shnerb, N. M. 2008. Origin of Pareto-like distributions in ecosystems.  
451 – *Phys. Rev. Lett.* 101: 268104.
- 452 24. Mendoza, F. et al. 2010. Multifractal properties of pore-size distribution in apple  
453 tissue using X-ray imaging. – *J. Food Eng.* 99: 206–215.

- 454 25. Meyer, H. A. 2006. Small-scale spatial distribution variability in terrestrial tardigrade  
455 populations. – *Hydrobiologia* 558: 133-139.
- 456 26. Murphy, R. J. et al. 2005. Remote-sensing of benthic chlorophyll: should ground-  
457 truth data be expressed in units of area or mass? – *J. Exp. Mar. Biol. Ecol* 316: 69–77
- 458 27. Murphy, R. J. et al. 2006. Quantitative imaging to measure photosynthetic biomass  
459 on an intertidal rock platform. – *Mar. Ecol. Prog. Ser.* 312: 45–55.
- 460 28. Murphy, R. J. et al. 2008. Field-based remote-sensing for experimental intertidal  
461 ecology: Case studies using hyperspatial and hyperspectral data for New South Wales  
462 (Australia). – *Remote Sens. Environ.* 112: 3353–3365
- 463 29. Murphy, R. J. et al. 2009. Field-based remote sensing of intertidal epilithic  
464 chlorophyll: techniques using specialized and conventional cameras. – *J. Exp. Mar. Biol.*  
465 *Ecol.* 380: 68–76.
- 466 30. Pascual, M. et al. 2002. Cluster size distributions: signatures of self-organization in  
467 spatial ecologies. – *Phil. Trans. R. Soc. Lond. B* 357: 657–666.
- 468 31. Potts, M. 1999. Mechanisms of desiccation tolerance in cyanobacteria. – *Eur. J.*  
469 *Phycol.* 34: 319–328.
- 470 32. Press, W. H. et al. 1992. *Numerical recipes in Fortran 77: the art of scientific*  
471 *computing*. 2<sup>nd</sup> edition. Volume 1 of Fortran numerical recipes. – Cambridge University  
472 Press, Cambridge, UK.
- 473 33. Rietkerk, M. et al. 2002. Self-Organization of Vegetation in Arid Ecosystems. – *Am.*  
474 *Nat.* 160(4): 524–530.
- 475 34. Rietkerk, M. and van de Koppel, J. 2008. Regular pattern formation in real  
476 ecosystems. – *Trends Ecol. Evol.* 23(3): 169-175.
- 477 35. Rodriguez, S. R. et al. 1993. Settlement of benthic invertebrates. – *Mar. Ecol. Prog.*  
478 *Ser.* 97: 193–207.

- 479 36. Saravia, L. A. et al. 2012. Multifractal growth in periphyton communities. – *Oikos*  
480 121: 1810–1820.
- 481 37. Scargle, J. D. 1982. Studies in astronomical time series analysis. II Statistical aspects  
482 of spectral analysis of unequally spaced data. – *Astrophys. J.* 263, 835–853.
- 483 38. Seuront, L. and Spilmont, N. 2002. Self-organized criticality in intertidal  
484 microphytobenthos patch patterns. – *Physica A* 313: 513–539.
- 485 39. Skov, M. W. et al. 2010. Past and present grazing boosts the photo-autotrophic  
486 biomass of biofilms. – *Mar. Ecol. Prog. Ser.* 401: 101–111.
- 487 40. Solé, R. V. and Bascompte, J. 2006. *Self-Organization in Complex Ecosystems.* –  
488 Princeton Univ. Press.
- 489 41. Stafford, R. and Davies, M.S. 2005. Spatial patchiness of epilithic biofilm caused by  
490 refuge-inhabiting high shore gastropods. – *Hydrobiologia* 545: 279–287.
- 491 42. Stanley, H. E. and Meakin, P. 1988. Multifractal phenomena in physics and  
492 chemistry. – *Nature* 335: 405–409.
- 493 43. Thompson, R. C. et al. 1999. Problems in extraction and spectrophotometric  
494 determination of chlorophyll from epilithic microbial biofilms: towards a standard method. –  
495 *J. Mar. Biol. Ass. UK* 79: 551–558.
- 496 44. Thompson, R. C. et al. 2000. Feast or famine for intertidal grazing molluscs: a  
497 mismatch between seasonal variations in grazing intensity and the abundance of microbial  
498 resources. – *Hydrobiologia* 440: 357–367.
- 499 45. Thompson, R. C. et al. 2004. Physical stress and biological control regulate the  
500 producer–consumer balance in intertidal biofilms. – *Ecology* 85: 1372–1382.
- 501 46. Underwood, A. J. 1984. Microalgal food and the growth of the intertidal gastropods  
502 *Nerita atramentosa* Reeve and *Bembicium nanum* (Lamarck) at four eights on a shore. – *J.*  
503 *Exp. Mar. Biol. Ecol.* 79:277-291.

- 504 47. van de Koppel, J. et al. 2005. Scale-dependent feedback and regular spatial patterns  
505 in young mussel beds. – *Am. Nat.* 165(3): E66–E77.
- 506 48. Vandermeer, J. et al. 2008. Clusters of ant colonies and robust criticality in a tropical  
507 agroecosystem. – *Nature* 451:457–459.
- 508 49. Weerman, E. J. et al. 2010. Spatial Self-Organization on Intertidal Mudflats through  
  
509 Biophysical Stress Divergence. – *Am. Nat.* 176(1): E15–E32.
- 510 50. Yang, J. and Wang, Y. T. 2013. Design of vascular networks: A mathematical  
511 approach. – *Int. J. Numer. Method Biomed. Eng.* 29(4): 515–529.
- 512 Supplementary material (Appendix oXXXXXX at <[www.oikosoffice.lu.se/appendix](http://www.oikosoffice.lu.se/appendix)>).  
513 Appendix 1–2–3–4.

514

515 Table 1.  $\beta$  coefficients and  $R^2$  from linear regressions of the power spectrum of EMPB biomass  
516 against frequency of observation for the two sampling dates.  $\beta$ s were estimated within the range of  
517 frequencies defined by the Nyquist and  $-7$  (on the natural logarithm scale). All the coefficients were  
518 significantly different from zero ( $p < 0.001$ ).

Transect	Series	January 2012		November 2012	
		$\beta$ (SE)	$R^2$	$\beta$ (SE)	$R^2$
1 (8 m)	1	1.22 (0.010)	0.79	1.02 (0.006)	0.80
	2	1.24 (0.008)	0.80	1.08 (0.005)	0.79
	3	1.33 (0.010)	0.78	0.95 (0.005)	0.79
2 (8 m)	1	1.17 (0.007)	0.82	1.61 (0.006)	0.83
	2	1.25 (0.007)	0.82	1.43 (0.006)	0.83
	3	1.24 (0.007)	0.79	1.59 (0.007)	0.81
3 (4 m)	1	1.55 (0.009)	0.77	1.39 (0.008)	0.81
	2	1.56 (0.011)	0.74	1.45 (0.009)	0.78
	3	1.64 (0.009)	0.80	1.45 (0.009)	0.80

519

520 Table 2. Mixed effect model on  $D_I$  spatial series calculated for 128 by 128 pixels plots extracted

521 from the two 8 m transects at each sampling date.

522 \*,  $p < 0.05$

<b>Fixed effects</b>		
		<i>Coefficient (SE)</i>
Intercept:	$\gamma_{00}$	1.9203 (0.0162)
Snail number	$\gamma_{01}$	$0.052 \cdot 10^{-3}$ (0.0002)
Pit number	$\gamma_{02}$	$-8.92 \cdot 10^{-3}$ (0.0124)
Rainfall	$\gamma_{03}$	$-0.008 \cdot 10^{-3}$ (0.0001)
Snail number x Pit number	$\gamma_{04}$	$0.055 \cdot 10^{-3}$ (0.0002)
Snail number x Rainfall	$\gamma_{05}$	$-0.007 \cdot 10^{-3}$ (0.00001) *
Pit number x Rainfall	$\gamma_{06}$	$0.001 \cdot 10^{-3}$ (0.00001)

<b>Random Effects</b>		
		<i>Variances</i>
Transect	$\sigma^2_{01}$	0.0003
Residual	$\sigma^2_e$	0.0022



523

524 LEGEND TO FIGURES

525 Figure 1. Sampling within transects. **A**, a section of a transect obtained from the merging of  
526 individual photos. The white chalk marks at the corners of each plot and the reflectance standard are  
527 visible in all the photos. **B** and **C**, spatial arrangement of sampled pixels. Crosses show the position  
528 of chalk marks that were used to align overlapping photos. Vertical black and grey dotted lines  
529 delimit the margins of the right-hand and left-hand photos in each pair of adjacent photos and define  
530 the region of overlap. Circles represent the reflectance standard. **B**, horizontal black lines represent  
531 the three series of observations used in  $1/f$  noise analysis that were aligned along a common  $y$   
532 coordinate; data from pixels in the overlapping regions (horizontal grey lines) were not used in the  
533 analysis; size of gaps in the region of overlap is measured in pixels. **C**, spatial arrangement along a  
534 common  $y$  coordinate of the five adjacent plots (128 by 128 pixels each) used in the multifractal  
535 analysis (black quadrates). Grey quadrates within regions of overlap have not been used in the  
536 analysis.

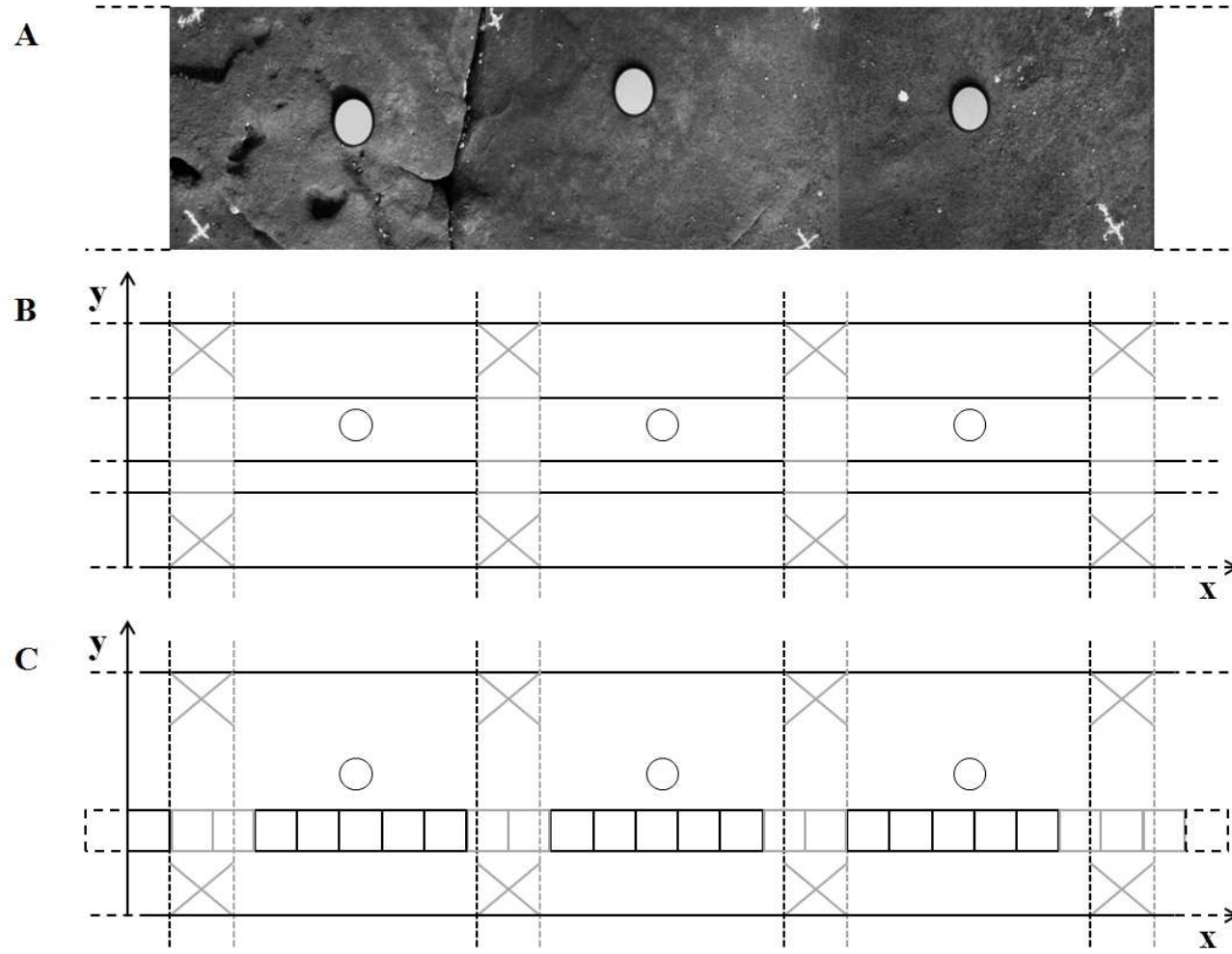
537 Figure 2. Calibration curve: chlorophyll  $a$  concentration determined from laboratory analysis  
538 ( $\mu\text{g}\cdot\text{cm}^{-2}$ ) versus image estimates of chlorophyll from sandstone cores (Ratio Vegetational Index,  
539 RVI),  $R^2=0.80$ ,  $SE=0.12$ ,  $p<0.001$ ,  $n=100$ .

540 Figure 3. Spectrum of generalized dimensions  $D_q$  versus  $q$  obtained for the 1024 by 1024 sampled  
541 plots separately for transect 1, 8 m long,  $n=11$  (A), transect 2, 8 m long,  $n=18$  (B) and transect 3, 4  
542 m long,  $n=10$  (C).

543 Figure 4. Interactive effect of the snails density and average rainfall in the week before the sampling  
544 on mean  $D_I$  ( $n=64$ , means  $\pm$  standard errors). White, average rainfall: 0 mm; gray, average rainfall:  
545 110 mm.

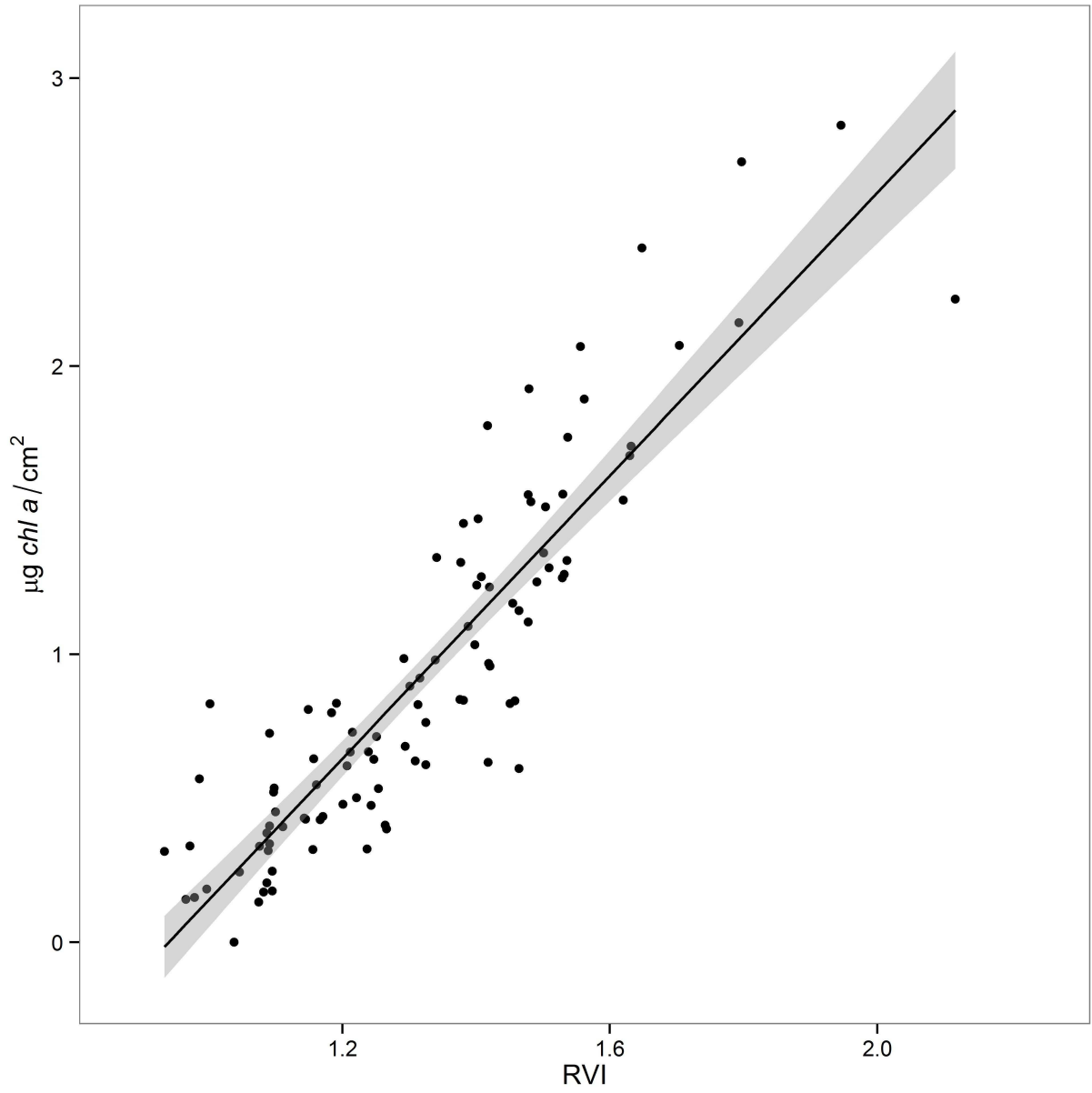
546 Figure 5. Spatial cross-correlation between littorinid density and  $D_I$  in each of two 8m transects  
547 sampled in January 2012 (A, B) and November 2012 (C, D).  $D_I$  values have been obtained from 64  
548 quadrats of 128 x 128 pixels aligned along a common y coordinate, but unevenly spaced along each  
549 transect. Note that these quadrats did not span the entire length of a transect as a consequence of  
550 avoiding portions of substratum that would have resulted in non-sense measures of EMPB biomass  
551 (e.g., shaded areas due to crevices).





Dal Bello et al. Figure 1.



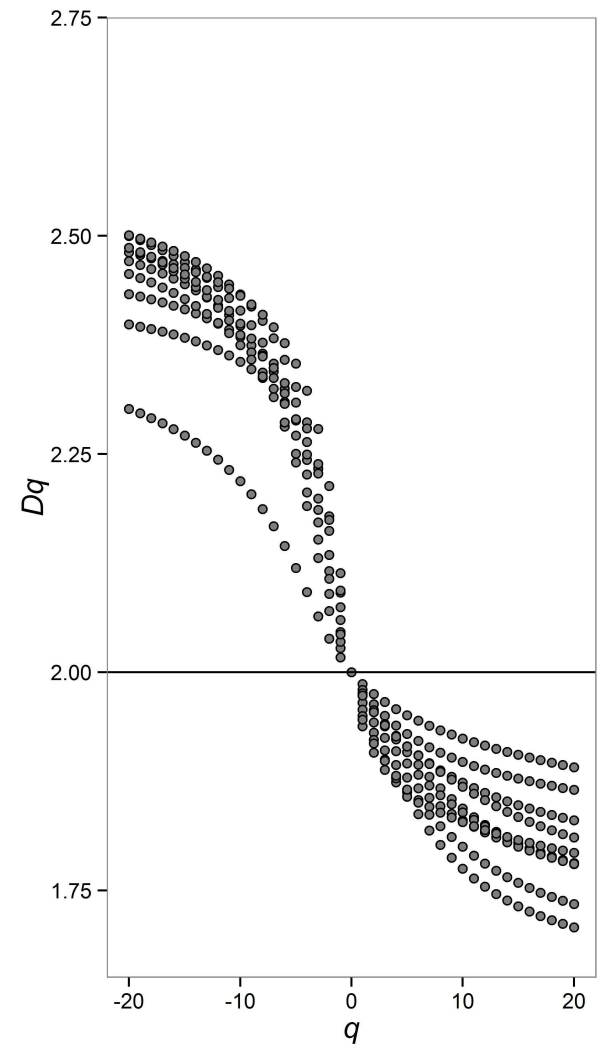
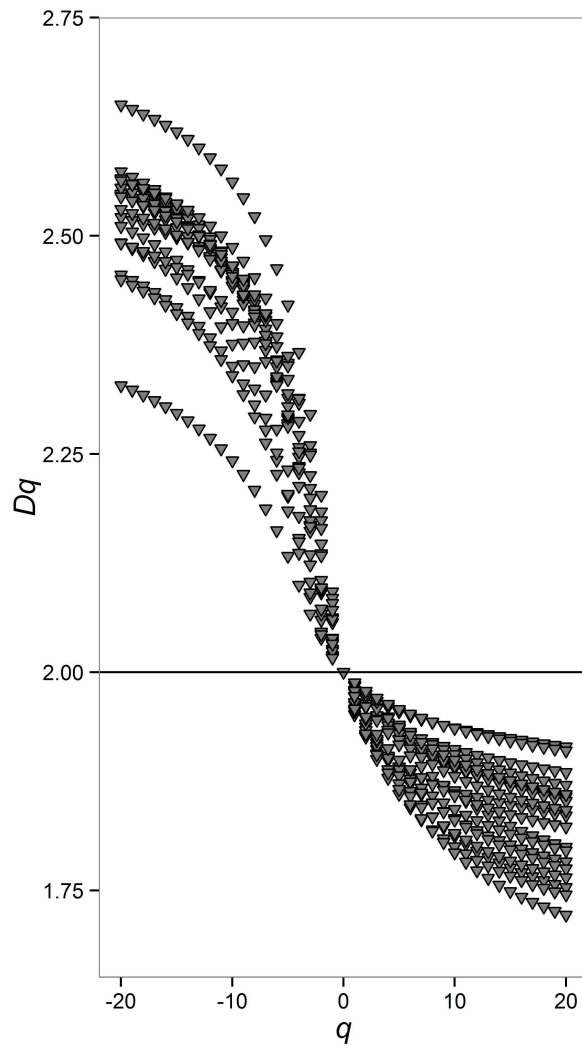
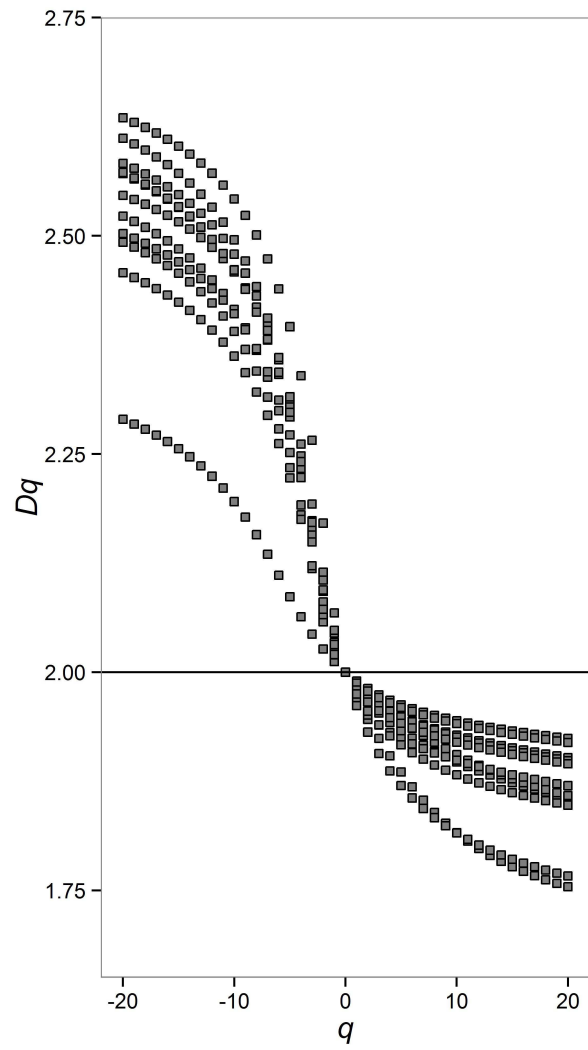


557

558

Dal Bello et al. Figure 2.





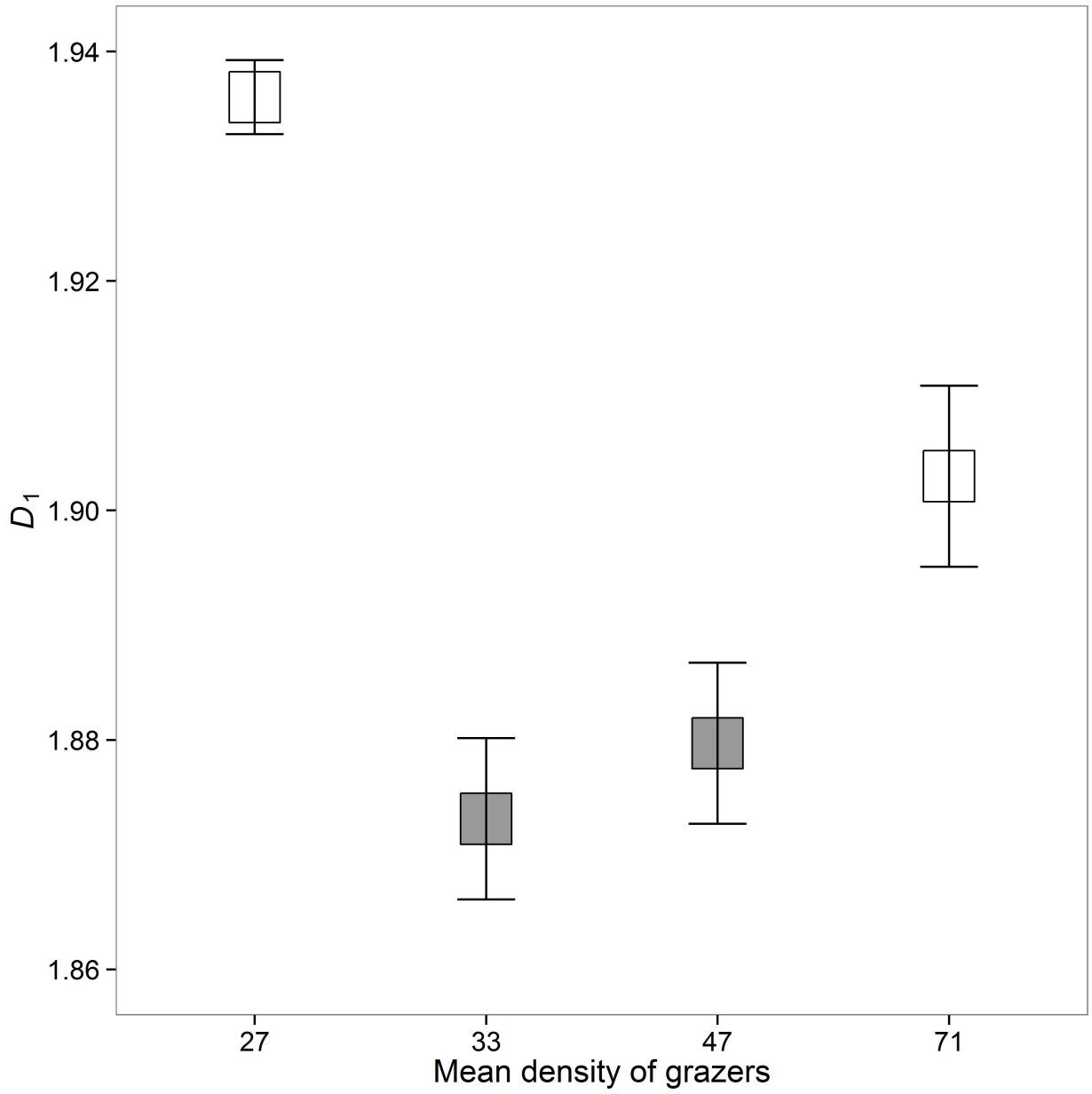
560

561

Dal Bello et al. Figure 3.



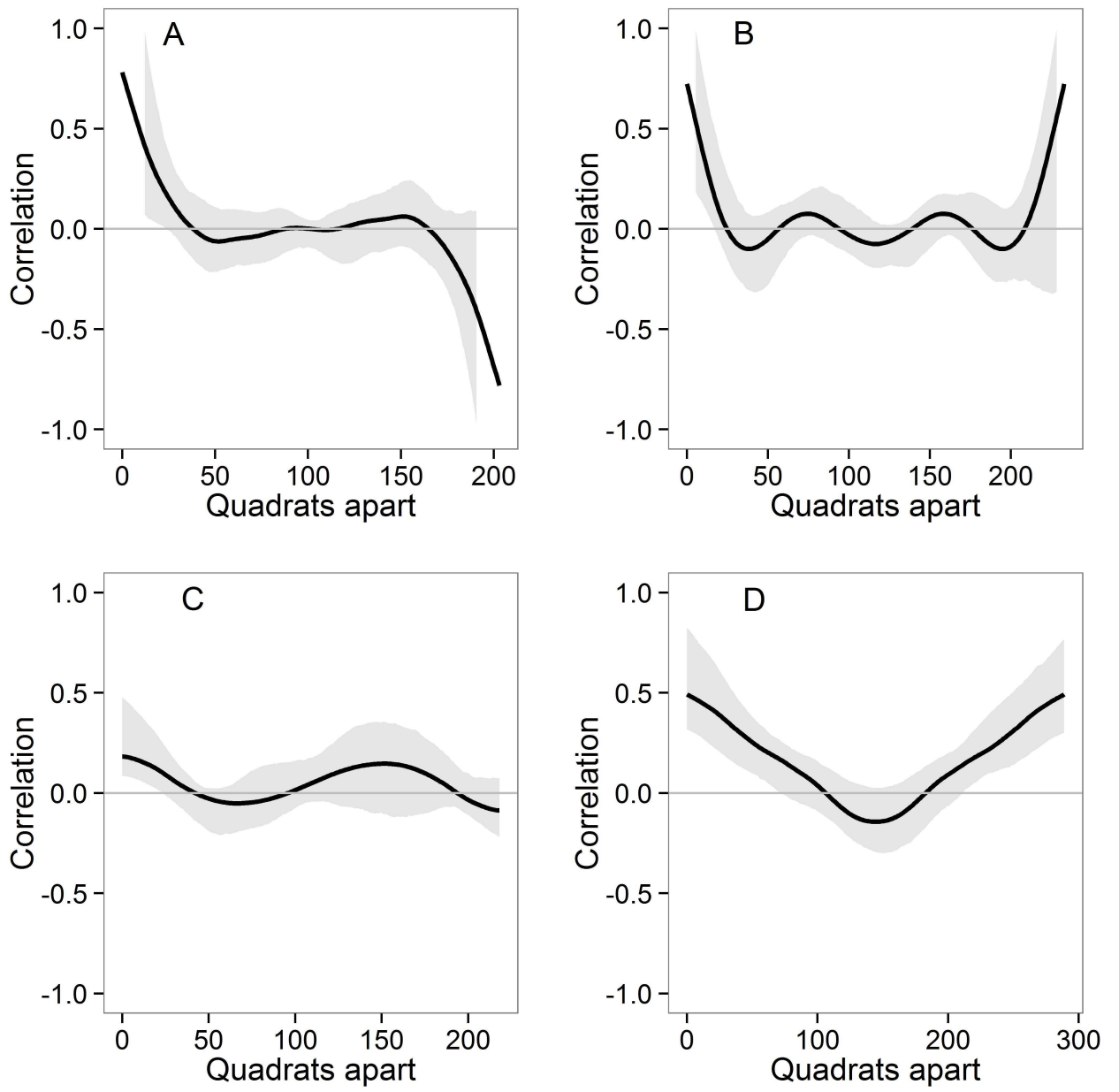




563

564

Dal Bello et al. Figure 4.



566  
567

568

Dal Bello et al. Figure 5.

569

## 570 **Appendix 1.**

### 571 **Calibration of data to reflectance**

572 Pixel values (Digital Number, *DN*) over the calibration standard are averaged and the reflectance ( $\rho$ )  
573 for each band in each photo is calculated as

$$574 \quad \rho(\text{photo}) = \frac{DN(\text{photo})\rho(\text{panel})}{DN(\text{panel})}$$

575 where  $\rho(\text{photo})$  is the reflectance at each pixel in the photo;  $\rho(\text{panel})$  is the reflectance of the

576 calibration standard, which is a known constant;  $DN(\text{photo})$  is *DN* at each pixel in the photo and

577  $DN(\text{panel})$  is the average *DN* of the pixels over the calibration standard (Murphy et al. 2006).

578 Calibration is part of a java-routine on ImageJ program with which each ADC-photo is processed.

579 Calibration of data to reflectance is of fundamental importance when one wants to compare

580 chlorophyll amounts estimated from photos acquired at different times and places.

### 581 **References**

582 Murphy, R. J. et al. 2006. Quantitative imaging to measure photosynthetic biomass on an intertidal

583 rock platform. – Mar. Ecol. Prog. Ser. 312: 45–55.

584

## 585 **Appendix 2**

### 586 **Calculation of the generalized dimension spectrum $D_q$**

587 Generalized dimensions are exponents estimated by the box counting method: the plot is covered  
 588 with a grid of  $N(\varepsilon)$  squares of side  $\varepsilon$  and for each square a value of standardized biomass is  
 589 calculated as

$$590 \quad M_i(q, \varepsilon) = \frac{(\mu_i(\varepsilon))^q}{\sum_j^{N(\varepsilon)} (\mu_j(\varepsilon))^q} \quad (1)$$

591 where  $\mu$  is the measured biomass and  $q$  is called the moment order and can be considered an  
 592 arbitrary exponent. An adjustment corresponding to  $+(\text{minimum observed biomass})/100$  has been  
 593 applied to all biomass values before the standardization in order to avoid zeros.

594 Then the partition function is computed as:

$$595 \quad Z_q(\varepsilon) = \sum_i^{N(\varepsilon)} (M_i(q, \varepsilon))^q \quad (2)$$

596 The operation is performed for different values of  $\varepsilon$  and  $q$ . In order to exactly divide the plots, a  
 597 grid size range of  $\varepsilon$  in power of two with a minimum of  $2^2=4$  and a maximum of  $2^7=128$  or  
 598  $2^{10}=1024$  pixels was chosen; the  $q$  exponent ranged between -20 and +20.

599 The generalized dimension is calculated as:

$$600 \quad D_q = \frac{1}{q-1} \lim_{\varepsilon \rightarrow 0} \frac{\log(Z_q(\varepsilon))}{\log \varepsilon} \quad (3)$$

601 This limit cannot be determined. Hence the second term in  $D_q$  is calculated as the slope of the  
 602 regression of  $\log(Z_q)$  versus  $\log(\varepsilon)$ . A linear relation is assumed, which is estimated using the least  
 603 squares method.

604 For  $q=1$ , the denominator of the first term in  $D_q$  is undefined, so Eq. 3 is replaced by:

605 
$$\lim_{\varepsilon \rightarrow 0} \frac{\sum_i^{N(\varepsilon)} \mu_i(\varepsilon) \log(\mu_i(\varepsilon))}{\log \varepsilon}$$

606 (4)

607 To see that  $D_q$  is actually an exponent, Eq. 3 can be rearranged to obtain:

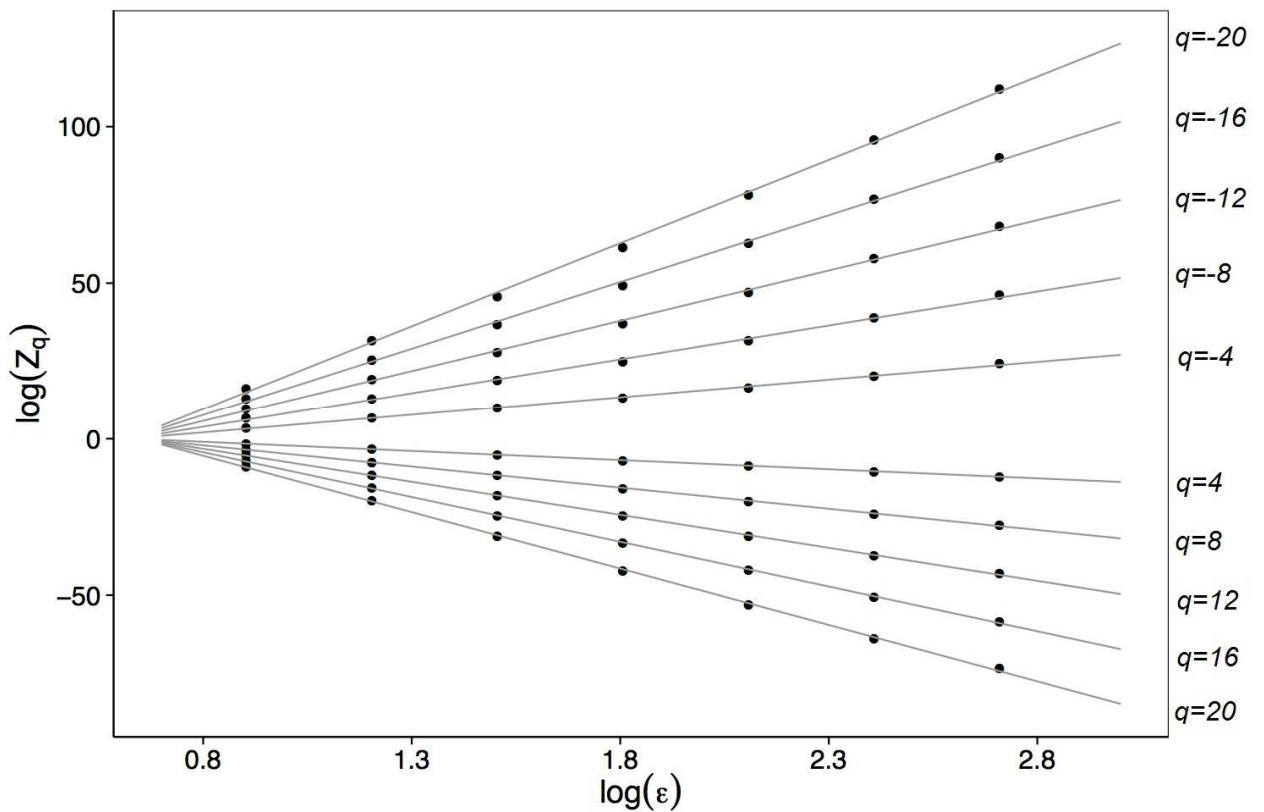
608 
$$Z_q \approx \varepsilon^{D_q(q-1)}$$

609 (5)

610 Eq. 5 determines how  $Z_q$  varies with the scale  $\varepsilon$  and it is evident that it is a power law.

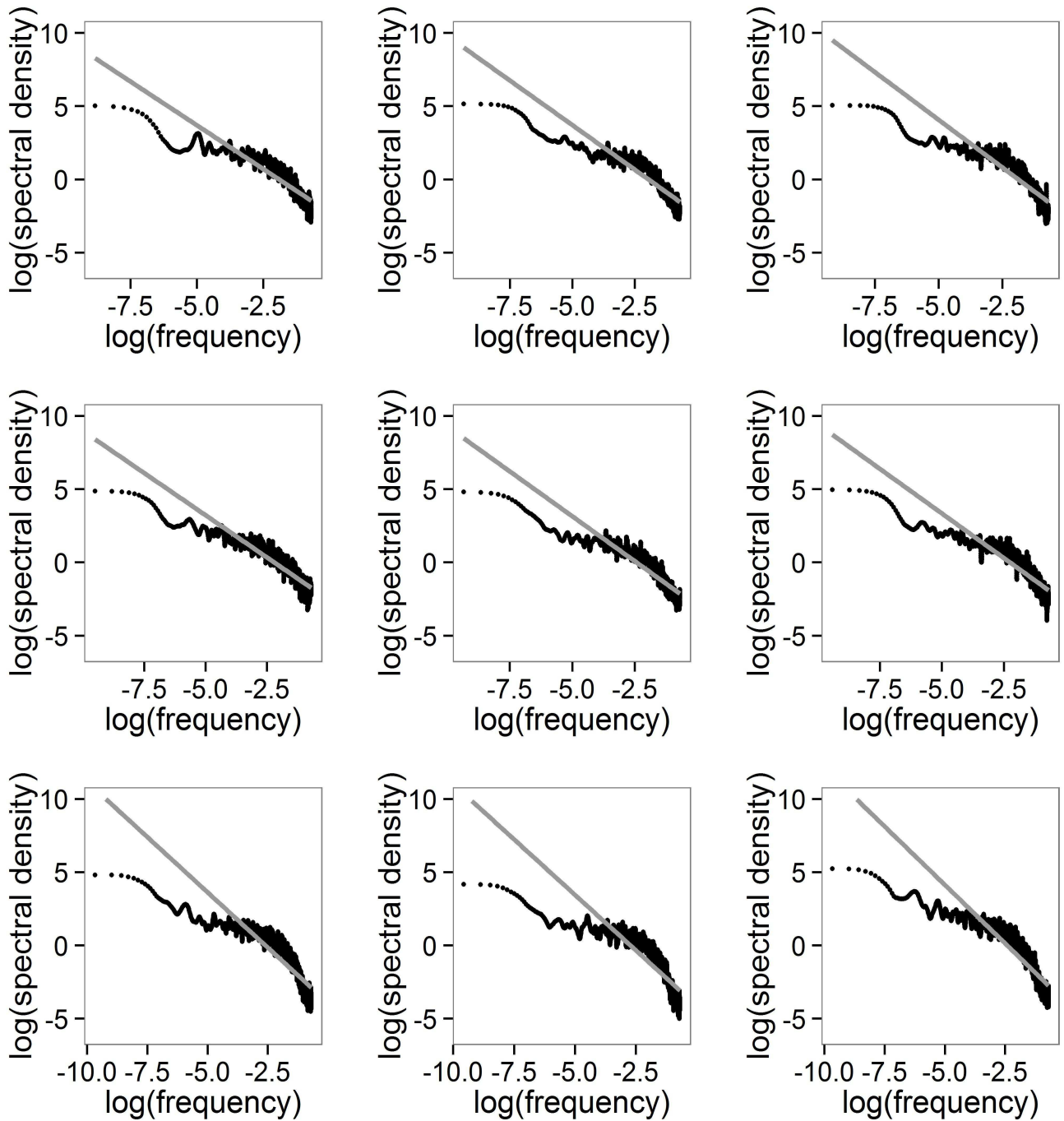
611 **Details of results**

612 We found a linear relation between  $\log(Z_q)$  and  $\log(\varepsilon)$  for all plots sampled and all  $q$  used. As a  
 613 measure of goodness of fit, we calculated the coefficient of determination  $R^2$ , which was always  
 614 larger than 0.99.



615

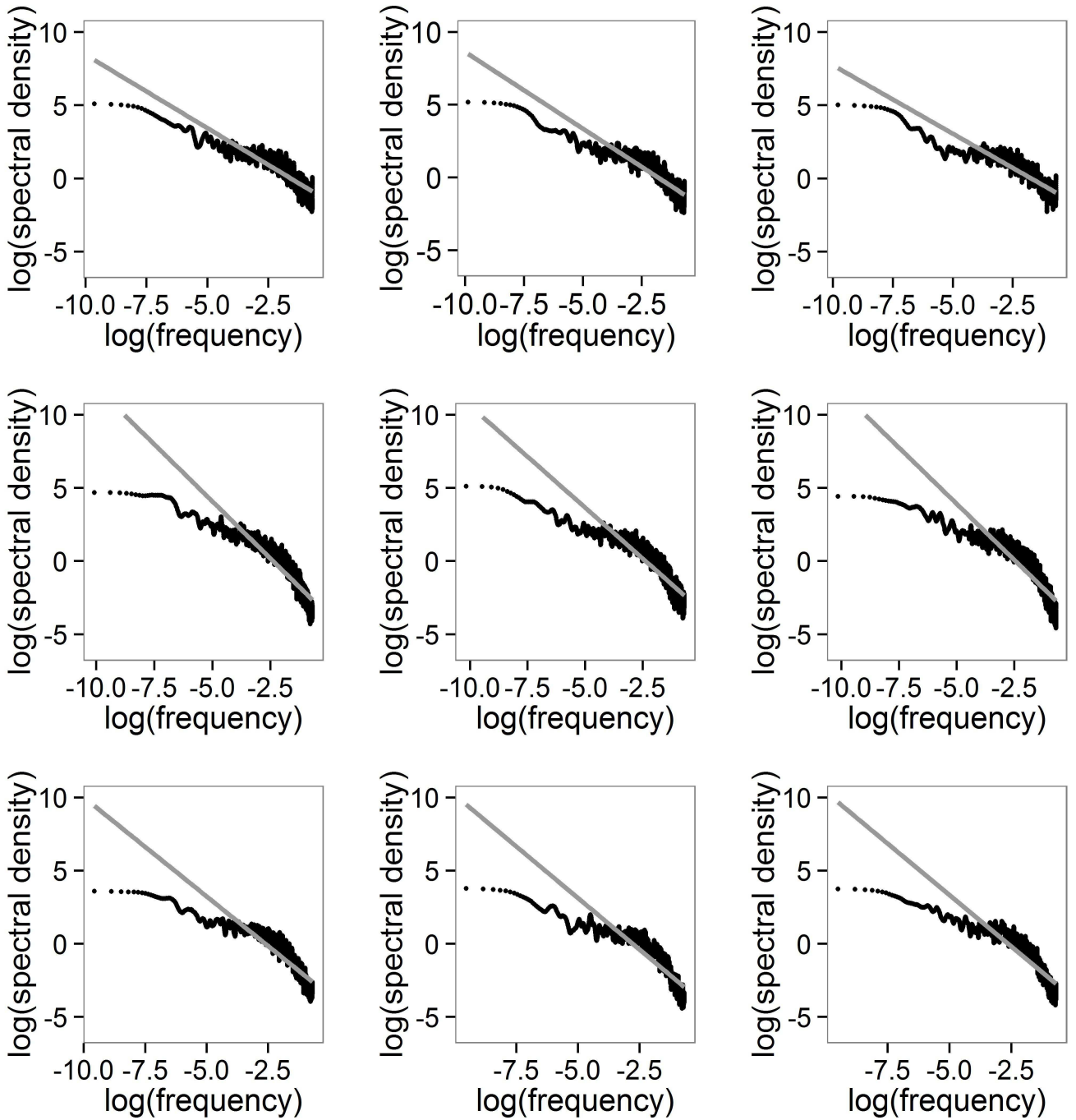
616 Figure A2.1. Example of a typical graph for the determination of the generalized dimension  $D_q$  for  
 617 one subplot 1024 by 1024 pixels. It shows all the regression lines for ten values of  $q$ .



620

621 Figure A3.1. Power spectra of EMPB biomass separately for each transect. **The spectral density is**622 **plotted against frequency of observation ( $\text{pixel}^{-1}$ ) on a natural log-log scale.** Data are from the first

623 date of sampling (26.01.2012).



624

625 Figure A3.2. Power spectra of EMPB biomass separately for each transect. The spectral density is

626 plotted against frequency of observation ( $\text{pixel}^{-1}$ ) on a natural log-log scale. Data are from the

627 second date of sampling (16.11.2012).



628

629 **Appendix 4**

630 Table A4.1.  $\beta$  coefficients and  $R^2$  from linear regressions of the power spectrum of EMPB biomass  
631 data obtained from quadrats of 80 x 80 pixels against frequency of observation for the two sampling  
632 dates. All the coefficients were significantly different from zero ( $p < 0.001$ ).

633

Transect	Series	January 2012		November 2012	
		$\beta$ (SE)	$R^2$	$\beta$ (SE)	$R^2$
1	1	1.71 (0.050)	0.92	0.88 (0.036)	0.80
	2	1.29 (0.058)	0.82	0.97 (0.033)	0.88
2	1	1.11 (0.034)	0.90	0.76 (0.045)	0.66
	2	1.35 (0.039)	0.91	0.86 (0.045)	0.71
3	1	1.17 (0.070)	0.72	1.36 (0.052)	0.86
	2	1.27 (0.050)	0.77	1.16 (0.054)	0.81

634